



Article

Controlled Magnetic Isolation and Decoupling of Perpendicular FePt Films by Capping Ultrathin Cu(002) Nano-Islands

Da-Hua Wei ^{1,*} , Ji-Hong Chang ^{1,†}, Chi-Chun Hsu ^{1,†}, Cheng-Jie Yang ^{1,†}, Yuan-Chang Liang ^{2,*},
Chung-Li Dong ^{3,*} and Yeong-Der Yao ^{4,*}

¹ Institute of Manufacturing Technology, Department of Mechanical Engineering, National Taipei University of Technology (TAIPEI TECH), Taipei 10608, Taiwan; ylsh159753@gmail.com (J.-H.C.); martin851017@gmail.com (C.-C.H.); bruce.60705@gmail.com (C.-J.Y.)

² Department of Optoelectronics and Materials Technology, National Taiwan Ocean University, Keelung 20224, Taiwan

³ Department of Physics, Tamkang University, Tamsui 25137, Taiwan

⁴ Institute of Physics, Academia Sinica, Taipei 11529, Taiwan

* Correspondence: dhwei@ntut.edu.tw (D.-H.W.); yuanvictory@gmail.com (Y.-C.L.); cldong@mail.tku.edu.tw (C.-L.D.); ydyao@phys.sinica.edu.tw (Y.-D.Y.)

† Contributed equally to this work.

Abstract: This study investigated the ultrathin Cu(002) capping nano-island effects on the magnetic characterizations and microstructure of epitaxial FePt(001) films directly fabricated on MgO(001) substrates at the relatively low temperature of 300 °C via electron-beam deposition. The enhancement of the coercivity is attributed to the lowered exchange coupling of FePt magnetic grains that begun from Cu atom behavior of spreading in many directions mainly along grain boundaries due to its lower surface energy than that of pure Fe or Pt. The measurement of angular-dependent coercivity shows a tendency of a domain-wall motion shift toward the rotation of the reverse-domain type upon the thickness of the Cu capping nano-island layer atop the FePt films. The intergranular interaction was clarified by the Kelly–Henkel plot, which indicated that there was strong exchange coupling (positive δM) between neighboring grains in the FePt continuous films without Cu capping nano-islands. On the other hand, a negative δM value was gained when the FePt films were capped with a Cu(002) single layer, indicating that the Cu capping layer can be used to control the strength of intergrain exchange coupling between the adjacent FePt grains and thicker Cu(002) capping nano-islands toward magnetic isolation; thus, there was an existence of dipole interaction in our designed Cu/FePt composite structure of stacked films.

Keywords: FePt; epitaxial multilayer films; ultrathin Cu(002) capping nano-island; magnetic decoupling/isolation; angular-dependent coercivity; Kelly–Henkel plot



Citation: Wei, D.-H.; Chang, J.-H.; Hsu, C.-C.; Yang, C.-J.; Liang, Y.-C.; Dong, C.-L.; Yao, Y.-D. Controlled Magnetic Isolation and Decoupling of Perpendicular FePt Films by Capping Ultrathin Cu(002) Nano-Islands. *J. Compos. Sci.* **2021**, *5*, 140. <https://doi.org/10.3390/jcs5060140>

Academic Editor:
Francesco Tornabene

Received: 1 April 2021
Accepted: 7 May 2021
Published: 21 May 2021

Publisher's Note: MDPI stays neutral with regard to jurisdictional claims in published maps and institutional affiliations.



Copyright: © 2021 by the authors. Licensee MDPI, Basel, Switzerland. This article is an open access article distributed under the terms and conditions of the Creative Commons Attribution (CC BY) license (<https://creativecommons.org/licenses/by/4.0/>).

1. Introduction

FePt $L1_0$ ordered (CuAu (I)-type) phase has undergone a fast and uninterrupted growth in recent years due to its excellent material properties containing mainly of high magnetocrystalline anisotropy constant ($K_u \sim 10^8$ erg/cm³), high saturation magnetization ($M_s \sim 1100$ emu/cc), high-anisotropy field ($H_a \sim 120$ kOe), high-energy products $(BH)_{max}$, high Curie temperature ($T_c \sim 480$ °C), and high environmental stability [1–8]. Mostly, the properties of high K_u Fe-based alloys could delay the problem of superparamagnetic effect and maintain enough thermal stability to overcome thermal fluctuation, even with a stable particle size down to the nanometer scale, which means these alloys have future potential applications, such as in excited spin ensemble of high-density electronic devices and magnetic recording media with storage densities surpassing 10 Tbits/in² [9–12]. The formation of the ordered FePt state requires high-temperature treatment (usually more than 500 °C), such as substrate heating during phase deposition or post-deposition annealing, to

overcome the activation energy from a metastable/disordered face-centered cubic (fcc) to an ordered face-centered tetragonal (fct) $L1_0$ phase transformation. The ferromagnetic, ordered phase usually showed a high exchange-coupled interaction between the neighboring grains due to the large-grain growth during the thermal process. Thus, the nanocomposite and nanogranular ferromagnetic film structures fabricated at low-temperature conditions have attracted significant attention because of the decoupling of the intergranular interaction that could enhance the signal-to-noise ratio; therefore, they are considered more favorable for the next generation magnetic storage media [13–23]. Many attempts have been made to propose the effect of top or under layers; the additive effect of metal oxides and nitride elements is a successful method to control the chemical ordering, microstructure, magnetic coupling, and crystalline orientation of the $L1_0$ magnetic thin films to meet the requirements of industrial manufacture, especially in technologically important perpendicular magnetic materials for multifunctional device applications [24–42]. Recently, the spin Hall effect (SHE)-induced perpendicular magnetization reversal behavior is with pay significant attention due to its potential for future low-power memory and logic devices. So, the spin Hall systems and related perpendicular magnetic tunnel junctions could pave the way towards more actual spin-orbit torque-based non-volatile magnetic memory and strain-spin coupling for applications of programmable logic devices [36–39,42].

Maeda et al. reported that the Fe-Pt-Cu ternary film could be obtained by the sputtering method. They found that FePt and Cu could form a solid solution in the Fe-Pt-Cu film and supposed that the addition of Cu into FePt matrix caused the enhancement of a driving force of the disorder–order transformation, resulting in the ordered behavior occurring at 300 °C, but so far, they have not provided any explanation for this obtained result [43–45]. On the other hand, Cu addition into the FePt films has been proposed not only to lower the ordering temperature, but also to change the preferred orientation with magnetic anisotropy from a perpendicular to parallel film direction [46–48].

The aim of this work is to control the intergrain interaction and maintain perpendicular anisotropy of the FePt films by introducing the Cu capping layer atop the FePt films. This present study also shows a significant effect in Cu/FePt composite system via different thicknesses of the Cu capping nano-island layer on the magnetic performance and microstructure at the relatively low deposition temperature of 300 °C. The corresponding intergranular exchange decoupling and magnetization reversal behavior of the designed Cu/FePt composite structure of stacked films were also systematically explored.

2. Experiments and Composite Film Structures

FePt-ordered structures composed of [Fe (0.5 nm)/Pt (0.5 nm)]₁₆ multilayer films were prepared by an electron-beam deposition system (homemade) directly onto the MgO(001) single-crystal substrates without any buffer layer under a vacuum of 6.67×10^{-6} Pa. The ultrathin Cu capping layer was deposited atop the [Fe/Pt]₁₆ bilayers, and its thickness was varied from 1 nm to 4 nm. All films were deposited at a relatively low temperature of 300 °C with a deposition rate of around 0.02 nm/s. The deposition method of Fe/Pt multilayers selected in this work was chosen in order to reduce the diffusion length of Fe and Pt atoms into the $L1_0$ lattice, whose concept is like the atomic arrangement in the unit cell with an artificial atomic-scale deposition [49–51]. The chemical composition of the binary phase was identified to be Fe₄₈Pt₅₂ by field emission electron probe X-ray microanalysis (FE-EPMA, JEOL, Tokyo, Japan). The crystalline structure was characterized by X-ray diffraction (XRD, PANalytical, Almelo, The Netherlands) with Cu K_α radiation ($\lambda = 1.54 \text{ \AA}$). In the XRD measurement with the proportional counter, the receiving slit was set to 0.1 mm, and the time per step was 3 s with a scan speed of $0.01^\circ 2\theta/s$. The microstructure of the films was observed by the Zeiss Supra field emission-scanning electron microscope (FE-SEM, Dresden, Germany), equipped with an Oxford Instruments NordlysNano™ camera. The scan area was $3 \times 3 \mu\text{m}^2$ and the beam was moved in a step size of 10 nm, so that it could provide a sufficient number of grains for the initial estimate of grain size. The grain size distribution and grain orientation distribution were

quantitatively measured with a plane-view microstructure. The magnetic properties were measured at room temperature by using a vibrating sample magnetometer (VSM, Lake Shore 7400, Westerville, OH, USA) with a maximum applied field of 20 kOe. The following analyses are focused on the pure FePt film structures without and with a Cu capping layer (with different thicknesses) in order to study the Cu capping nano-island layer effect on the magnetization reversal mechanism and microstructure of the FePt continuous films.

3. Results and Discussion

Figure 1 shows the FE-SEM surface morphologies of the FePt films (a) without and (b) with a 2-nm and (c) a 4-nm Cu capping nano-island layer taken by secondary electron image (SEI) mode, respectively. The corresponding backscattering electron image (BEI) image taken from (c) is shown in Figure 1d. Pure FePt film without the Cu capping layer was connected, and the structure looks like a continuous film, as shown in Figure 1a. The surface morphology of the FePt films with the 2-nm and 4-nm Cu capping nano-island layer show the Cu nano-islands on top of the FePt films, as shown in Figure 1b,c, respectively. From the comparison of the SEI and BEI images shown in Figure 1c,d, it was found that the Cu(002) nano-islands stand on top of the FePt films, consistent with the XRD results, which are discussed and shown in Figure 2. The formation of nanogranular Cu grains with the (002) preferred crystallographic orientation is confirmed and shown in Figure 1d. Cu anisotropic rectangular-like nano-islands were alignment with the direction of MgO [100] and with the (002) preferred orientation, and the primary facet planes were (100) and (010), as shown in Figure 1d. Shown in Figure 1e are the FePt films with the 4-nm Cu capping nano-island layer, and the corresponding Figure 1f image is the element mapping of Cu in the selected area for Figure 1e. Furthermore, the local analysis of composition by energy dispersion spectroscopy (EDS) revealed that the Cu/FePt composite-structured film is uniform. The above results indicate that some of the Cu nano-islands persist on the top of FePt when the nominal thickness of Cu is 2 nm, while they could partially penetrate into the FePt layer, resulting in the lattice deformation of FePt structures consistent with the broad results of the rocking curves of the FePt(001) superlattice peak. The surface energy of Cu (1.9 Jm^{-2}) is much lower than that of pure Fe (2.9 Jm^{-2}) and Pt (2.7 Jm^{-2}) [52]. This indicates that Cu atoms could easily diffuse into the FePt magnetic grains along the grain boundaries and create a strain-energy modulability at the interface due to its much lower surface energy than that of pure Fe or Pt.

Figure 2 shows the in-plane XRD patterns for $[\text{Fe}/\text{Pt}]_{16}$ film structures (a) without and (b) with a 2-nm-thick and (c) a 4-nm-thick Cu capping nano-island layers, respectively. Figure 2d–f are the corresponding slow scan curves of the FePt(002) and Cu(002) peaks in the θ - 2θ scan of Figure 2a–c, respectively. Apart from the primary (002) and (004) peaks, (001) and (003) superlattice peaks of the $L1_0$ -ordered FePt compound were clearly seen for all films. The unlabeled sharp peaks are due to the MgO substrate. Only (00 n) diffraction peaks in Figure 2 were shown in the whole diffraction patterns (θ - 2θ scan) with a wide scanning range, indicating that all the FePt films without and with a Cu capping nano-island layer were strongly textured to the (001) planes, and also confirming that the stacked film structures epitaxially formed on the MgO substrate. The intensities of the fundamental (002) and (001) superlattice peaks of the FePt maintained almost constant for FePt films without and with a Cu capping layer, indicating the ordering degree of Cu/FePt composite structured film is not influenced by the Cu capping nano-island layer. It has been demonstrated that the disorder–order transformation is dominantly controlled by the growth process of $L1_0$ -ordered domains [53]. The activation energy in the FePt thin film plays the role of the driving force, not only for grain growth, but also for disorder–order transformation. Thus, the grain growth will be suppressed by the $L1_0$ -ordering process. On the other hand, it has been reported that the ordering process of FePt-based thin films could be controlled by atom diffusion [54]. The intensity of the Cu(002) diffraction peak got stronger with the increasing Cu capping layer thickness, indicating that the Cu capping layer is stand on top of the FePt films. On the other hand, the full width

at half maximum (FWHM) value slightly increased with increasing thickness of the Cu capping layer, indicating that the lattice deformation of the FePt films is induced by inhomogeneous solidification of Cu due to immiscibility of Cu in the FePt phase. The results mentioned above imply that Cu atoms tend to diffuse into the FePt films through the grain boundary to slightly broaden the rocking curve of FePt(001). In this work, the effects of an ultrathin Cu(002) capping nano-island layer on the magnetic behavior and corresponding magnetization reversal mechanism of FePt(001) films was demonstrated and compared, because no other fabrication condition in our designed Cu/FePt composite structure of stacked films was changed except for the pure FePt multilayer film structures without and with a single Cu capping nano-island layer.

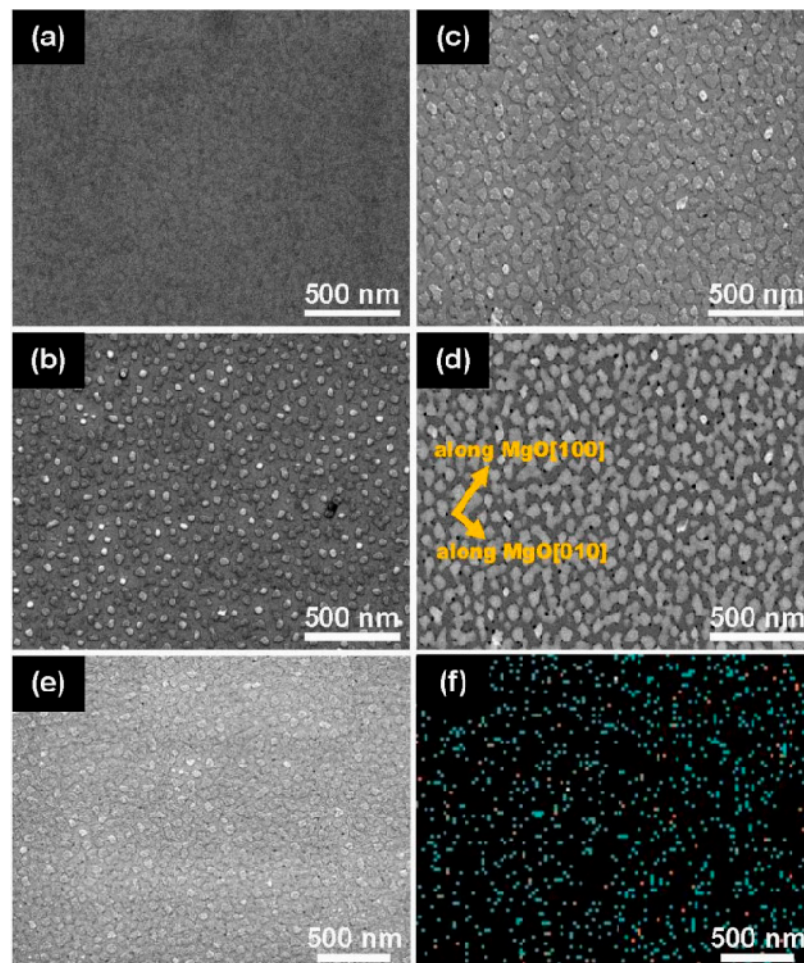


Figure 1. FE-SEM surface morphologies of the FePt multilayer films (a) without and (b) with a 2-nm and (c) a 4-nm Cu capping nano-island layer taken by secondary electron image (SEI) mode, respectively. The corresponding backscattering electron image (BEI) image taken from (c) is (d). (e) The 4-nm Cu capping nano-island layer taken by SEI mode, and (f) is the element mapping of Cu nano-island atop the FePt films.

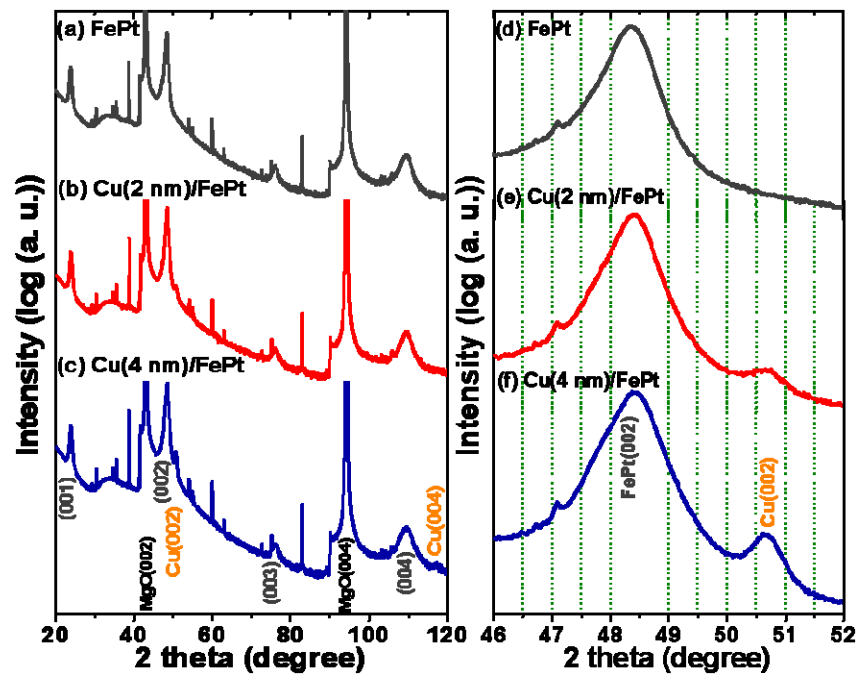


Figure 2. X-ray diffraction patterns ($\theta-2\theta$ scans) for the FePt multilayer films (a) without and (b) with a 2-nm and (c) a 4-nm Cu capping nano-island layer, respectively. The (d–f) are the corresponding slow scan curves of the FePt(002) and Cu(002) peaks in the $\theta-2\theta$ scan of (a–c), respectively.

The perpendicular and parallel hysteresis loops for FePt multilayer films without and with a single 4-nm-thick Cu capping layer are shown in Figure 3a,b, respectively. The magnetic easy axis was constantly perpendicular to the film plane, and the perpendicular anisotropy was apparent for all films. The corresponding magnetic measurement including out-of-plane coercivity ($H_{c\perp}$), saturation magnetization ($M_{s\perp}$), and remanent squareness ratio ($M_{r\perp}/M_{s\perp}$) values as a function of the Cu capping nano-island thickness over FePt films are listed in Table 1 in detail. The coercivity value of the FePt thin films increased from 3020 Oe (without Cu) to 4500 Oe (4 nm Cu). The saturation magnetization ($M_{s\perp}$) and remanent squareness ratio ($M_{r\perp}/M_{s\perp}$) values both decreased with the increasing thickness of the Cu capping layer and ranged from 915 emu/cm³ (without Cu) to 805 emu/cm³ (4 nm Cu) and 0.98 (without Cu) to 0.9 (4 nm Cu), respectively. The decrease of the squareness ratio may support that the intergranular interactions of FePt are less magnetically coupled with the addition of the Cu capping nano-island layer and may indicate that some Cu atoms penetrated into FePt magnetic grains through the grain boundary to decouple the intergranular interaction between the FePt neighboring magnetic grains, thus enhancing coercivity of Cu/FePt composite structure with stacked films. The intergranular exchange coupling, magnetic reversal mechanism, and the corresponding magnetic characterizations of the designed Cu/FePt composite-structured films are compared and discussed below.

Table 1. Out-of-plane coercivity ($H_{c\perp}$), saturation magnetization ($M_{s\perp}$), and remanent squareness ratio ($M_{r\perp}/M_{s\perp}$) values for the FePt multilayer structures without and with an ultrathin single 1-, 2- and 4-nm Cu capping nano-island layer, respectively.

Cu Thickness (nm)	$H_{c\perp}$ (Oe)	$M_{s\perp}$ (emu/cm ³)	$M_{r\perp}/M_{s\perp}$ (ratio)
0	3020	915	0.98
1	3100	890	0.96
2	3300	852	0.94
4	4500	805	0.90

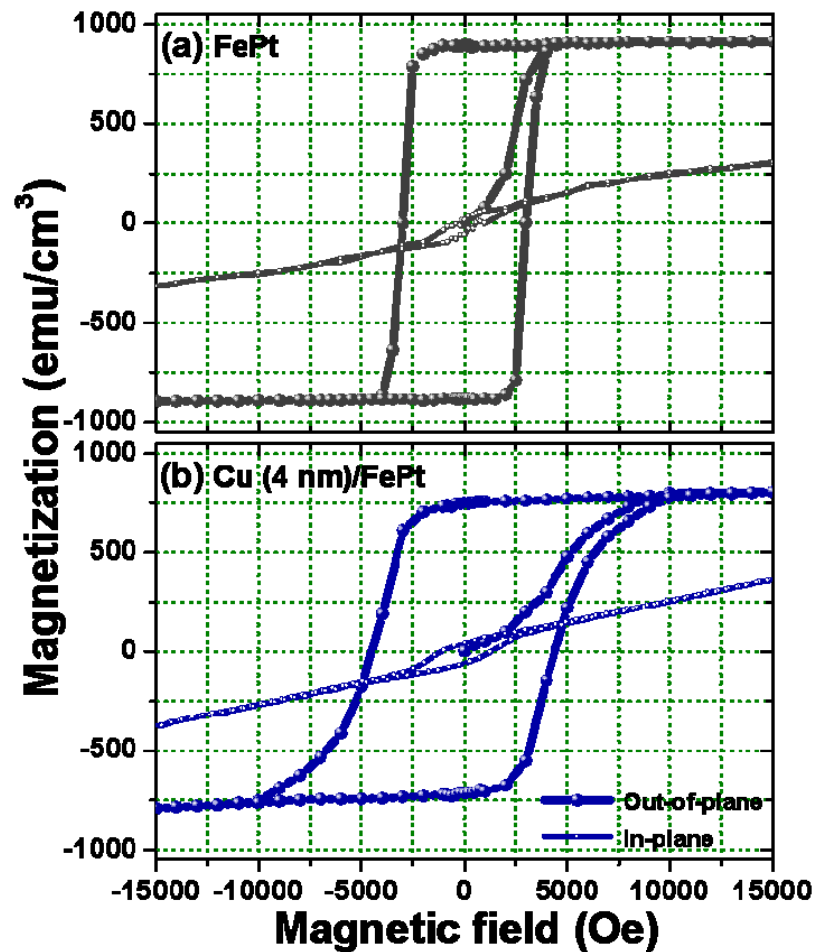


Figure 3. The perpendicular and parallel hysteresis loops of the FePt multilayer films (a) without and (b) with a single 4-nm-thick Cu capping nano-island layer, respectively.

The angular dependence of coercivity has been given to explore the magnetization reversal behavior of the FePt films without and with 1-nm, 2-nm, and 4-nm-thick Cu capping layers, as shown in Figure 4. Shown in Figure 4 are the perfectly theoretical curves, defining two boundary conditions of domain-wall motion and rotation of the Stoner–Wohlfarth (S–W) models, respectively. For a perfect domain-wall motion model, the coercivity at the angle θ is proportional to $1/\cos(\theta)$, where θ is the angle between the applied field and easy axis of the uniaxial magnetic anisotropy. As for the S–W model with rotation mechanism, the variation of the coercivity decreases with increasing θ . The angular dependence of the coercivity profile for the FePt without Cu show displayed a typical peak behavior due to the continuous film morphology of the pure FePt multilayers. In this article, the alignment of the easy-axis perpendicular to film plane is belonging to the domain walls Bloch-like. This significantly enhances the propagation of the domain walls while the morphology of pure FePt film is continuous. When the FePt films were capped with a Cu single nano-island layer, the profile was more nearby to the rotation mode as the thickness of Cu capping layer increased, and the magnetization reversal behavior become more independent. The above results demonstrate an inclination in progress lessened domain-wall motion behavior, but a raised rotation mode mechanism in the magnetization reversal process via the addition of a Cu single layer atop the FePt multilayer films, which may decouple the intergranular interaction between the FePt neighboring magnetic grains. According to the results mentioned above, the magnetization reversal mechanism of the Cu/FePt composite system could be simply controlled by the thickness of a Cu single capping layer.

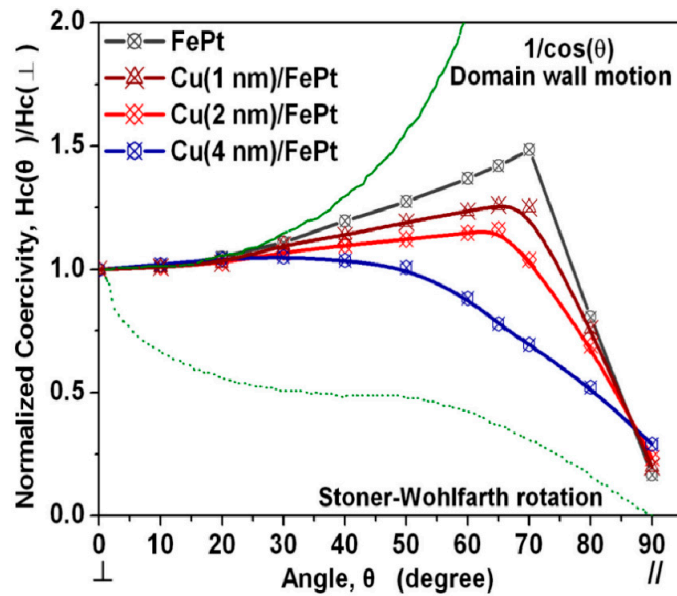


Figure 4. Angular dependence of coercivity for the FePt multilayer films without and with 1-, 2- and 4-nm-thick Cu capping nano-island layers, respectively. The angle refers to that between the easy axis (film normal) and the applied magnetic field direction.

Figure 5 shows a Kelly–Henkel plot (δM measurement) for the FePt multilayer films without and with 1-nm, 2-nm and 4-nm-thick Cu capping layers, respectively. The δM measured mode is used to identify the intergranular interaction in magnetic materials, which is defined as [55]:

$$\delta M = M_{DCD}(H) - [1 - 2M_{IRM}(H)], \tag{1}$$

where $M_{DCD}(H)$ and $M_{IRM}(H)$ are the normalized dc-demagnetization remanence and isothermal remanence as a function of the applied magnetic field, respectively. The positive δM peak indicates ferromagnetic intergranular interactions. On the other hand, the negative δM peak exhibits dipole intergranular interactions associated with incoherent rotation. It can be seen from Figure 5 that FePt films without Cu addition indicated a positive δM value (strong ferromagnetic interaction), while FePt films with the Cu capping layer exhibited only the negative δM value at all applied magnetic fields (dipole interaction). This suggests that the independent moment rotation of the FePt films is due to the Cu atoms being partially penetrated into FePt magnetic grains through the grain boundary, resulting in the degradation of exchange intergranular interactions between neighboring magnetic grains. The important parameter δM value is well known to decide the noise of magnetic recording media; this value can be controlled basically by the thickness of Cu capping layer in our designed Cu/FePt composite system, which determines the intergranular interaction for the magnetic composite system.

The normalized initial magnetization curve shown in Figure 6 could be used to explain the magnetization reversal mechanism for the FePt multilayer films without and with a 4-nm-thick Cu capping nano-island layer. The FePt films with a single Cu capping layer became much harder much more difficult to reach saturation magnetization compared to that of the pure FePt films at the same applied magnetic field. This could be understood if the magnetization reversal behavior was dominated by pinning sites, as the domain-wall movement would not shift unless the external applied magnetic field was greater than the pinning field. If the magnetization reversal behavior is more near to the rotation of the Stoner–Wohlfarth (S–W) mode, the single domain magnetic grains only reverse their magnetization behavior when the external applied magnetic field surpasses the anisotropy energy [56–60]. So, the pure FePt multilayer films without a single Cu capping layer shows

near to the nucleation type of the initial magnetization curves, and the FePt multilayer films with a single Cu capping layer shows near to the typical pinning type of the initial magnetization curve.

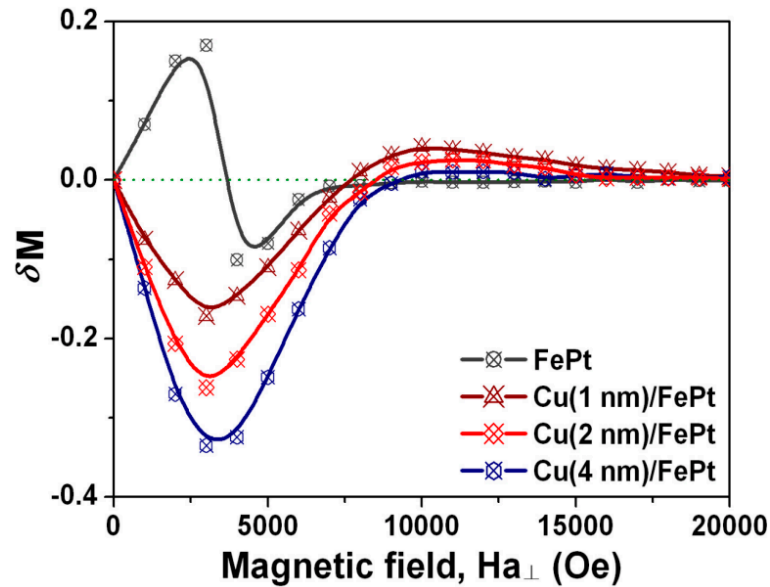


Figure 5. δM curves of the FePt multilayer films without and with 1-, 2- and 4-nm-thick Cu capping nano-island layers with the external field applied perpendicular to the film plane direction.

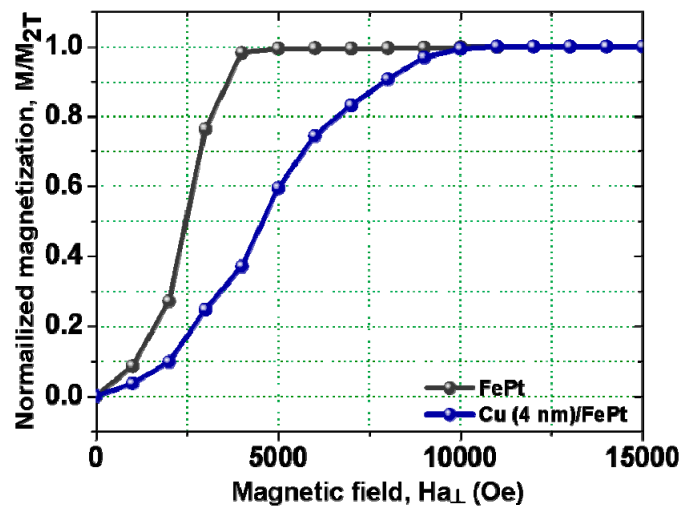


Figure 6. Initial magnetization curves for the FePt multilayer films without and with a 4-nm-thick Cu capping nano-island layer. The magnetic field was applied in the perpendicular direction to the multilayer films.

FePt alloy films fabricated at room temperature tend to act as a disordered ($A1$) phase with a low cubic magnetocrystalline anisotropy. The accomplishment of the ordered ($L1_0$) phase usually requires high-temperature processing (beyond $500\text{ }^\circ\text{C}$), which normally leads to grain growth and resolution reduction of the magnetic force microscope (MFM) measurement. Thus, the challenge is to obtain a hard and isotropic-like FePt layer on the MFM probe at a low temperature (below $500\text{ }^\circ\text{C}$). Our work presents the way that a Cu capping nano-island layer atop the FePt films is different from the method of co-sputtering or the co-evaporation technique, and better to keep the c -axis highly oriented and perpendicular to the film plane at the reduced temperature of $300\text{ }^\circ\text{C}$, which is suitable

for future applications in high-density perpendicular recording media and FePt-based MFM probes.

4. Conclusions

In this article, a straightforward and simple approach is presented, which showed that an ultrathin Cu single nano-island layer capped on top of the FePt multilayer films could reduce the intergranular exchange coupling and, thus, enhance the coercivity at the relatively low deposition temperature of 300 °C. From the angular dependence of coercivity measurement revealed that with the increased thickness of a single Cu capping layer atop the FePt multilayer films, the magnetization reversal mechanism was observed to shift from the domain-wall motion behavior to be closer to the rotation mode dominated in the Cu/FePt composite films. Thus, the FePt alloy film with a single Cu capping nano-island layer is effective to enhance coercivity, reduce the intergranular coupling strength, and lower media noise, which will be of great aid in the development for modern applications of ultrahigh-density perpendicular spin electronic nanodevices.

Author Contributions: Conceptualization, D.-H.W. and Y.-D.Y.; methodology, D.-H.W.; software, D.-H.W., J.-H.C., C.-C.H., C.-J.Y.; validation, D.-H.W.; formal analysis, D.-H.W.; investigation, D.-H.W. and Y.-D.Y.; resources, Y.-D.Y.; data curation, D.-H.W. and Y.-D.Y.; writing—original draft preparation, D.-H.W.; writing—review and editing, D.-H.W. and Y.-D.Y.; visualization, D.-H.W.; supervision, D.-H.W. and Y.-D.Y.; project administration, D.-H.W. and Y.-D.Y.; funding acquisition, D.-H.W., Y.-C.L., C.-L.D. and Y.-D.Y. All authors have read and agreed to the published version of the manuscript.

Funding: This research was funded by Ministry of Science and Technology (MOST), through Grants number 110-2731-M-027-001 and 108-2628-E-027-002-MY3 and University System of Taipei Joint Research Program through Grants No. USTP-NTUT-NTOU-106-03 and USTP-NTUT-NTOU-107-05.

Acknowledgments: The authors acknowledge financial support of the main research projects of the Ministry of Science and Technology (MOST) under Grant Nos. 110-2731-M-027-001 and 108-2628-E-027-002-MY3. Da-Hua Wei greatly appreciates the financial support of the University System of Taipei Joint Research Program (Grant Nos. USTP-NTUT-NTOU-106-03 and USTP-NTUT-NTOU-107-05).

Conflicts of Interest: The authors declare no conflict of interest.

References

1. Weller, D.; Moser, A.; Folk, L.; Best, M.E.; Lee, W.; Toney, M.F.; Schwickert, M.F.; Thiele, J.U.; Doerner, M.F. High K_u materials approach to 100 Gbits/in². *IEEE Trans. Magn.* **2000**, *36*, 10–15. [[CrossRef](#)]
2. Ravindran, P.; Kjekshus, A.; Fjellvåg, H.; James, P.; Nordström, L.; Johansson, B.; Eriksson, O. Large magnetocrystalline anisotropy in bilayer transition metal phases from first-principles full-potential calculations. *Phys. Rev.* **2001**, *63*, 144409. [[CrossRef](#)]
3. Albrecht, M.; Rettner, C.T.; Moser, A.; Best, M.E.; Terris, B.D. Recording performance of high-density patterned perpendicular magnetic media. *Appl. Phys. Lett.* **2002**, *81*, 2875. [[CrossRef](#)]
4. Yan, M.L.; Powers, N.; Sellmyer, D.J. Highly oriented nonepitaxially grown $L1_0$ FePt films. *J. Appl. Phys.* **2003**, *93*, 8292. [[CrossRef](#)]
5. Shima, T.; Takanashi, K.; Takahashi, Y.K.; Hono, K. Coercivity exceeding 100 kOe in epitaxially grown FePt sputtered films. *Appl. Phys. Lett.* **2004**, *85*, 2571. [[CrossRef](#)]
6. Wang, J.P. Tilting for the top. *Nat. Mater.* **2005**, *4*, 191. [[CrossRef](#)]
7. Thomson, T.; Hu, G.; Terris, B.D. Intrinsic distribution of magnetic anisotropy in thin films probed by patterned nanostructures. *Phys. Rev. Lett.* **2006**, *96*, 257204. [[CrossRef](#)]
8. Chappert, C.; Fert, A.; van Dau, F.N. The emergence of spin electronics in data storage. *Nat. Mater.* **2007**, *6*, 813–823. [[CrossRef](#)]
9. Seki, T.; Hasegawa, Y.; Mitani, S.; Takahashi, S.; Imamura, H.; Maekawa, S.; Nitta, J.; Takanashi, K. Giant spin Hall effect in perpendicularly spin-polarized FePt/Au devices. *Nat. Mater.* **2008**, *7*, 125–129. [[CrossRef](#)]
10. Wei, D.H.; Yao, Y.D. Controlling microstructure and magnetization process of FePd (001) films by staged thermal modification. *Appl. Phys. Lett.* **2009**, *95*, 172503–1–172503–3. [[CrossRef](#)]
11. Vogler, C.; Abert, C.; Bruckner, F.; Suess, D.; Praetorius, D. Heat-assisted magnetic recording of bit-patterned media beyond 10 Tb/in². *Appl. Phys. Lett.* **2016**, *108*, 102406. [[CrossRef](#)]
12. Wu, C.; Jiang, Y.; Niu, Z.; Zhao, D.; Pei, W.; Wang, K.; Wang, Q. Effects of high magnetic field annealing on FePt nanoparticles with shape-anisotropy and element-distribution-anisotropy. *RSC Adv.* **2021**, *11*, 10463–10467. [[CrossRef](#)]
13. Lee, H.S.; Bain, J.A.; Laughlin, D.E. Use of bias sputtering to enhance decoupling in oxide composite perpendicular recording media. *Appl. Phys. Lett.* **2007**, *90*, 252511. [[CrossRef](#)]

14. Wu, Y.C.; Wang, L.W.; Lai, C.H. Low-temperature ordering of (001) granular FePt films by inserting ultrathin SiO₂ layers. *Appl. Phys. Lett.* **2007**, *91*, 072502. [[CrossRef](#)]
15. Chen, J.S.; Lim, B.C.; Hu, J.F.; Liu, B.; Chow, G.M.; Ju, G. Low temperature deposited L1₀ FePt–C (001) films with high coercivity and small grain size. *Appl. Phys. Lett.* **2007**, *91*, 132506. [[CrossRef](#)]
16. Seki, T.; Yako, H.; Yamamoto, T.; Kubota, T.; Sakuraba, Y.; Takanashi, K. Spin torque-induced magnetization dynamics in giant magnetoresistance devices with Heusler alloy layers. *J. Phys. D Appl. Phys.* **2015**, *48*, 164010-1–164010-8. [[CrossRef](#)]
17. Dong, K.F.; Deng, J.Y.; Peng, Y.G.; Ju, G.; Chow, G.M.; Chen, J.S. Columnar structured FePt films epitaxially grown on large lattice mismatched intermediate layer. *Sci. Rep.* **2016**, *6*, 34637. [[CrossRef](#)]
18. Li, W.; Chen, L. Grain growth mechanism and magnetic properties in L1₀-FePt thin films. *AIP Adv.* **2017**, *7*, 085203. [[CrossRef](#)]
19. Zhang, Y.; Kalitsov, A.; Ciston, J.; Mryasov, O.; Ozdol, B.; Zhu, J.; Jain, S.; Zhang, B.; Livshitz, B.; Chernyshov, A.; et al. Microstructure and magnetic properties of ultrathin FePt granular films. *AIP Adv.* **2018**, *8*, 125018. [[CrossRef](#)]
20. Bello, F.; Sanvito, S.; Hess, O.; Donegan, J.F. Shaping and Storing Magnetic Data Using Pulsed Plasmonic Nanoheating and Spin-Transfer Torque. *ACS Photonics* **2019**, *6*, 1524–1532. [[CrossRef](#)]
21. Atkinson, L.J.; Evans, R.F.L.; Chantrell, R.W. Micromagnetic modeling of the heat-assisted switching process in high anisotropy FePt granular thin films. *J. Appl. Phys.* **2020**, *128*, 073907. [[CrossRef](#)]
22. Ito, K.; Hayashida, M.; Masuda, H.; Nishio, T.; Goto, S.; Kura, H.; Koganezawa, T.; Mizuguchi, M.; Shimada, Y.; Konno, T.J.; et al. Epitaxial L1₀-FeNi films with high degree of order and large uniaxial magnetic anisotropy fabricated by denitrating FeNiN films. *Appl. Phys. Lett.* **2020**, *116*, 242404. [[CrossRef](#)]
23. Suzuki, I.; Kubo, S.; Sepelri-Amin, H.; Takahashi, Y.K. Dependence of the Growth Mode in Epitaxial FePt Films on Surface Free Energy. *ACS Appl. Mater. Interfaces* **2021**, *13*, 16620–16627. [[CrossRef](#)]
24. Chen, J.S.; Lim, B.C.; Wang, J.P. Controlling the crystallographic orientation and the axis of magnetic anisotropy in L1₀ FePt films. *Appl. Phys. Lett.* **2002**, *81*, 1848. [[CrossRef](#)]
25. Takahashi, Y.K.; Hono, K. Interfacial disorder in the L1₀ FePt particles capped with amorphous Al₂O₃. *Appl. Phys. Lett.* **2004**, *84*, 383. [[CrossRef](#)]
26. Zhou, M.J.; Li, Q.; Yang, F.J.; Wang, H.B.; Wang, H.; Tang, D. Structure and magnetic properties of FePt/B₄C multilayer thin films: Role of the compositional elements intermixing. *Appl. Phys. Lett.* **2007**, *91*, 061920. [[CrossRef](#)]
27. Wei, D.H.; Yao, Y.D. Magnetization reversal mechanism and microstructure refinement of the FePt (001) nanogranular films With SiO₂ capping layer. *IEEE Trans. Magn.* **2009**, *45*, 4092–4095. [[CrossRef](#)]
28. Samal, S.; Kolinova, M.; Blanco, I. The magneto-mechanical behavior of active components in iron-elastomer composite. *J. Compos. Sci.* **2018**, *2*, 54. [[CrossRef](#)]
29. Li, H.; Li, X.; Kim, D.; Zhao, G.; Zhang, D.; Diao, Z.; Chen, T.; Wang, J.P. High spin polarization in epitaxial Fe₄N thin films using Cr and Ag as buffer layers. *Appl. Phys. Lett.* **2018**, *112*, 162407. [[CrossRef](#)]
30. Klein, T.; Wang, W.; Yu, L.; Wu, K.; Boylan, K.L.M.; Vogel, R.I.; Skubitz, A.P.N.; Wang, J.P. Development of a multiplexed giant magnetoresistive biosensor array prototype to quantify ovarian cancer biomarkers. *Biosens. Bioelectron.* **2019**, *126*, 301–307. [[CrossRef](#)]
31. Yamamoto, K.; Kubota, Y.; Suzuki, M.; Hirata, Y.; Carva, K.; Berritta, M.; Takubo, K.; Uemura, Y.; Fukaya, R.; Tanaka, K.; et al. Ultrafast demagnetization of Pt magnetic moment in L1₀-FePt probed by magnetic circular dichroism at a hard x-ray free electron laser. *New J. Phys.* **2019**, *21*, 123010. [[CrossRef](#)]
32. Zhou, W.; Seki, T.; Imamura, H.; Ieda, J.; Takanashi, K. Spinmotive force in the out-of-plane direction generated by spin wave excitations in an exchange-coupled bilayer element. *Phys. Rev. B* **2019**, *100*, 094424. [[CrossRef](#)]
33. Seki, T.; Iihama, S.; Taniguchi, T.; Takanashi, K. Large spin anomalous Hall effect in L1₀-FePt: Symmetry and magnetization switching. *Phys. Rev. B* **2019**, *100*, 144427. [[CrossRef](#)]
34. Thiruvengadam, V.; Singh, B.B.; Kojima, T.; Takanashi, K.; Mizuguchi, M.; Bedanta, S. Magnetization reversal, damping properties and magnetic anisotropy of L1₀-ordered FeNi thin films. *Appl. Phys. Lett.* **2019**, *115*, 202402. [[CrossRef](#)]
35. Saito, M.; Ito, H.; Suzuki, Y.; Mizuguchi, M.; Koganezawa, T.; Miyamachi, T.; Komori, F.; Takanashi, K.; Kotsugi, M. Fabrication of L1₀-FeNi by pulsed-laser deposition. *Appl. Phys. Lett.* **2019**, *114*, 072404. [[CrossRef](#)]
36. Liu, L.; Qin, Q.; Lin, W.; Li, C.; Xie, Q.; He, S.; Shu, X.; Zhou, C.; Lim, Z.; Yu, J.; et al. Current-induced magnetization switching in all-oxide heterostructures. *Nat. Nanotech.* **2019**, *14*, 939–944. [[CrossRef](#)]
37. Zhang, D.L.; Zhu, J.; Qu, T.; Lattery, D.M.; Victora, R.H.; Wang, X.; Wang, J.P. High-frequency magnetoacoustic resonance through strain-spin coupling in perpendicular magnetic multilayers. *Sci. Adv.* **2020**, *6*, eabb4607. [[CrossRef](#)]
38. Zhao, Z.; Smith, A.K.; Jamali, M.; Wang, J.P. External-field-free spin hall switching of perpendicular magnetic nanopillar with a dipole-coupled composite structure. *Adv. Electron. Mater.* **2020**, *6*, 1901368. [[CrossRef](#)]
39. Shu, X.; Zhou, J.; Deng, J.; Lin, W.; Yu, J.; Liu, L.; Zhou, C.; Yang, P.; Chen, J.S. Spin-orbit torque in chemically disordered and L1₁-ordered CuPt. *Phys. Rev. Mater.* **2020**, *3*, 114410. [[CrossRef](#)]
40. Chan, M.H.; Hsieh, M.R.; Liu, R.S.; Wei, D.H.; Hsiao, M. Magnetically guided theranostics: Optimizing magnetic resonance imaging with sandwich-like kaolinite-based iron/platinum nanoparticles for magnetic fluid hyperthermia and chemotherapy. *Chem. Mater.* **2020**, *32*, 697–708. [[CrossRef](#)]
41. Wang, X.; Krylyuk, S.; Josell, D.; Zhang, D.; Lyu, D.; Wang, J.P.; Gopman, D.B. Buffer layer engineering of L1₀ FePd thin films with large perpendicular magnetic anisotropy. *AIP Adv.* **2021**, *11*, 025106. [[CrossRef](#)]

42. Liu, L.; Zhou, C.; Shu, X.; Li, C.; Zhao, T.; Lin, W.; Deng, J.; Xie, Q.; Chen, S.; Zhou, J.; et al. Symmetry-dependent field-free switching of perpendicular magnetization. *Nat. Nanotech.* **2021**, *16*, 277–282. [[CrossRef](#)] [[PubMed](#)]
43. Maeda, T.; Kai, T.; Kikitsu, A.; Nagase, T. Akiyama, Reduction of ordering temperature of an FePt-ordered alloy by addition of Cu. *J. Appl. Phys. Lett.* **2002**, *80*, 2147–2149. [[CrossRef](#)]
44. Maeda, T.; Kikitsu, A.; Kai, T.; Nagase, T.; Aikawa, H.; Akiyama, J. Effect of added Cu on disorder-order transformation of $L1_0$ -FePt. *IEEE Trans. Magn.* **2002**, *38*, 2796–2798. [[CrossRef](#)]
45. Takahashi, Y.K.; Ohnuma, M.; Hono, K. Effect of Cu on the structure and magnetic properties of FePt sputtered film. *J. Magn. Mater.* **2002**, *246*, 259–265. [[CrossRef](#)]
46. Ding, Y.F.; Chen, J.S.; Liu, E. Controlling the crystallographic orientation and easy axis of magnetic anisotropy in $L1_0$ FePt films with Cu additive. *Surf. Coat. Technol.* **2005**, *198*, 270–273. [[CrossRef](#)]
47. Matsumoto, S.; Shima, T. Magnetic properties of FePt thin films with multilayered structure. *J. Phys. Conf. Ser.* **2011**, *266*, 012038. [[CrossRef](#)]
48. Lei, W.; Yu, Y.; Yang, W. Cu induced low temperature ordering of fct-FePtCu nanoparticles prepared by solution phase synthesis. *J. Mater. Chem. C* **2019**, *7*, 11632–11638. [[CrossRef](#)]
49. Chou, S.C.; Yu, C.C.; Liou, Y.; Yao, Y.D.; Wei, D.H.; Chin, T.S.; Tai, M.F. Annealing effect on the Fe/Pt multilayers grown on Al_2O_3 substrates. *J. Appl. Phys.* **2004**, *95*, 7276. [[CrossRef](#)]
50. Wei, D.H. Magnetic assemblies of FePt (001) nanoparticles with SiO_2 addition. *J. Appl. Phys.* **2009**, *105*, 07A715. [[CrossRef](#)]
51. Wei, D.H. Perpendicular magnetization behavior of low-temperature ordered FePt films with insertion of Ag nanolayers. *Materials* **2016**, *9*, 209. [[CrossRef](#)]
52. Himpel, F.J.; Ortega, J.E.; Mankey, G.J.; Willis, R.F. Magnetic nanostructures. *Adv. Phys.* **1998**, *47*, 511–597. [[CrossRef](#)]
53. Li, X.H.; Liu, B.T.; Li, W.; Sun, H.Y.; Wu, D.Q.; Zhang, X.Y. Atomic ordering kinetics of FePt thin films: Nucleation and growth of $L1_0$ ordered domains. *J. Appl. Phys.* **2007**, *101*, 093911. [[CrossRef](#)]
54. Vlasova, N.I.; Popov, A.G.; Shchegoleva, N.N.; Gaviko, V.S.; Stashkova, L.A.; Kandaurova, G.S.; Gunderov, D.V. Discovery of metastable tetragonal disordered phase upon phase transitions in the equiatomic nanostructured FePd alloy. *Acta Mater.* **2013**, *61*, 2560–2570. [[CrossRef](#)]
55. Kelly, P.E.; O’Grady, K.; Mayo, P.I.; Chantrell, R.W. Switching mechanisms in cobalt-phosphorus thin films. *IEEE Trans. Magn.* **1989**, *25*, 3881–3883. [[CrossRef](#)]
56. Wohlfarth, E.P. The coefficient of magnetic viscosity. *J. Phys. F: Met. Phys.* **1984**, *14*, L155. [[CrossRef](#)]
57. Gau, J.S.; Brucker, C.F. Angular variation of the coercivity in magnetic recording thin films. *J. Appl. Phys.* **1985**, *57*, 3988. [[CrossRef](#)]
58. Byun, C.; Sivertsen, J.M.; Judy, J.H. A study on magnetization reversal mechanisms of CoCr films. *IEEE Trans. Magn.* **1986**, *22*, 1155–1157. [[CrossRef](#)]
59. Suzuki, T.; Honda, N.; Ouchi, K. Magnetization reversal process in polycrystalline ordered Fe–Pt(001) thin films. *J. Appl. Phys.* **1999**, *85*, 4301. [[CrossRef](#)]
60. Coffey, K.R. Angle dependent magnetization reversal of thin film magnetic recording media. *J. Appl. Phys.* **2003**, *93*, 8471. [[CrossRef](#)]